Hindawi
Shock and Vibration
Volume 2020, Article ID 2841254, 11 pages
https://doi.org/10.1155/2020/2841254

Research Article

Research on NOFRF Entropy-Based Detection Method for Early Damage of Pillar Porcelain Insulator

Hanling Mao,[1] **Weili Tang**,[2] **Yingxiang Huang**,[3] **Hanying Mao**,[4] **Zhenfeng Huang**,[1] **and Xinxin Li**[1]

[1]*School of Mechanical Engineering, Guangxi University, Guangxi Key Laboratory of Manufacturing System and Advanced Manufacturing Technology, Nanning 530004, China*
[2]*College of Light Industry and Food Engineering, Guangxi University, Nanning 530004, China*
[3]*Nanning Railway Administration Quality and Technical Inspection Institute, Nanning 530005, China*
[4]*School of Mechanical and Transportation Engineering, Guangxi University of Science and Technology, Liuzhou 542506, China*

Correspondence should be addressed to Hanling Mao; maohl79@gxu.edu.cn, Hanying Mao; mhy2005516@sina.com, and Zhenfeng Huang; zfhuang@gxu.edu.cn

Received 20 November 2019; Accepted 25 April 2020; Published 6 July 2020

Academic Editor: Giuseppe Ruta

The pillar porcelain insulator is an important protection device that is related to the safety of the entire power grid. Small damage of it may even cause a disaster. Nonlinear output frequency response functions (NOFRFs) can well reflect the nonlinear characteristics of early damage in the system. This paper uses the NOFRF entropy-based harmonic excitation detection method to detect the damage of the structure. Its effect has been verified by using metal specimens. Then, the pulse hammer detection and harmonic detection are carried out to detect the early-stage damage of the pillar porcelain insulator, and they achieve a good result, which verifies that the harmonic detection method can detect the early-stage damage in the pillar porcelain insulator as well. In addition, the orthogonal test of the simulated breathing crack model is used to search the greatest influence of the parameters of crack on the detection index. Through the orthogonal analysis, the results show that among the lengths, positions, and angles of the crack, the length of crack is the main factor that affects the detection index.

1. Introduction

The pillar porcelain insulator is an insulating component that plays an important role in the power grid. During the service of the pillar porcelain insulator, cracks may occur due to the effects of wind load, sudden changes in temperature, and so on. The failure of the insulator would reduce the operational life of the entire line and even cause a disaster.

Therefore, it is of great practical significance to study the online detection for early damage of insulators. The acoustic detection, ultraviolet detection, and laser Doppler vibration method introduced in [1–3] have the advantages of good real-time performance and high efficiency, but there are still problems such as being susceptible to environmental influences and expensive equipment. Because of the global nature of vibration detection, the vibration-based method is convenient and effective to detect structural fatigue damage. Vibration detection is widely used in structural nondestructive testing in the fields of construction and machinery [4–6]. In [7, 8], the vibration detection method of the pillar insulator based on two kinds of detection standards of natural frequency variation and characteristic frequency energy amplitude transfer was introduced, and the feasibility of vibration detection was verified by experiments. Furthermore, to find the damage of the structures in the early stage, some scholars proposed the vibration detection method based on nonlinear features to detect damage in the system [7–10]. Now, nonlinear methods have become a research hotspot because nonlinear algorithms are more sensitive to changes in damage.

At present, there are many nonlinear analysis methods. The nonlinear output frequency response function (NOFRF)

is an effective nonlinear algorithm, which was derived from the Volterra series. The Volterra series is widely used for damage detection [11–13]. The concept of NOFRFs was proposed by Lang and Billings in recent years [14, 15]. Peng and Lang [16–18] had done much work which has shown that NOFRFs can effectively describe the nonlinearity of the system and characterize the nonlinear characteristics of the damage, especially the early stage of the damage. After that, Mao et al. [19, 20] proposed a NOFRF estimation method based on an improved algorithm for the NARMAX model with rectangular pulse hammer detection based on NOFRF theory and built several detection indexes based on NOFRFs, which used the concepts of information entropy, complexity, and divergence, respectively. Through the experiment, the analysis results show that the pulse hammer detection and proposed damage detection indexes have a good performance for indicating the degree of fatigue damage, especially the index which used the concept of information entropy. The pulse hammer can excite a wide frequency range, which has a good effect on NOFRF estimation. Liu et al. [21, 22] established a weighted contribution rate as an index for NOFRFs. The index values of the rotor with different crack relative depths were estimated. The extracted fault features are enlarged in the method, which can be used in the diagnosis of the early-stage crack of the rotor. Liu et al. [23] also proposed a variable weighted contribution rate of NOFRFs, which is sensitive to the slight misalignment of the rotor system.

However, when it comes to online monitoring, the shortcomings of the pulse hammer detection method are revealed. Pulse hammer excitation signal is not a continuous signal, so it is difficult to achieve real-time monitoring. Furthermore, in the actual detection process, the hammer excitation position and angle are difficult to control. So, a large number of repeated detections should be done to reduce the error.

In this work, a NOFRF entropy-based harmonic excitation detection method was used to detect the damage of the structure. Its detection efficiency is higher than that of pulse hammer detection, and the detection cost is cheap as well. Unlike the pulse signal, the harmonic signal is a continuous excitation signal, which is more beneficial to online monitoring. Then, the harmonic excitation detection and hammering excitation detection were performed on the same specimens. The results of them were compared to verify that harmonic excitation detection is effective in estimating the NOFRF entropy index. When its effectiveness had been proved, it was applied to the pillar porcelain insulator. Finally, the greatest influence of crack on values of NOFRF detection indexes was explored by simulation.

2. Theoretical Background

2.1. Nonlinear Output Frequency Response Function. NOFRFs were derived from the Volterra series. Each order of NOFRFs can be estimated by using the frequency spectra of excitation signal and response signal, which are used as input and output, respectively. The definition [14] is given as

$$G_n(j\omega) = \frac{\int_{-\infty}^{\infty} \cdots \int_{-\infty}^{\infty} H_n(j\omega_1, \ldots, j\omega_n) \prod_{i=1}^{n} U(j\omega_1) d\omega_1 \ldots d\omega_n}{\int_{-\infty}^{\infty} \cdots \int_{-\infty}^{\infty} \prod_{i=1}^{n} U(j\omega_1) d\omega_1 \ldots d\omega_n}, \quad 1 \le n \le N, \tag{1}$$

where $H_n(j\omega_1, \cdots, j\omega_n)$ is the n-th order generalized frequency response function (GFRF); $U(j\omega)$ is the input; and $Y(j\omega)$ is the output frequency response, which can be written as

$$Y(j\omega) = \sum_{n=1}^{N} Y_n(j\omega) = \sum_{n=1}^{N} G_n(j\omega) U_n(j\omega). \tag{2}$$

The above description can be expressed as Figure 1.

In Figure 1, $u^N(t)$ is the N power of $u(t)$.

$G_1(j\omega)$ represents the linear part of the system. And $G_2(j\omega)$, ..., $G_N(j\omega)$ represent the nonlinear parts of the system.

The general estimation method of NOFRFs was given by Peng and Lang [14] as follows.

If n sets of excitation signals and response signals are obtained, equation (3) can be obtained.

$$\begin{cases} Y_1(j\omega) = G_1(j\omega)\alpha_1 U_1^*(j\omega) + G_2(j\omega)\alpha_1^2 U_2^*(j\omega) + \cdots + G_n(j\omega)\alpha_1^n U_n^*(j\omega), \\ Y_2(j\omega) = G_1(j\omega)\alpha_2 U_1^*(j\omega) + G_2(j\omega)\alpha_2^2 U_2^*(j\omega) + \cdots + G_n(j\omega)\alpha_2^n U_n^*(j\omega), \\ \vdots \\ Y_n(j\omega) = G_1(j\omega)\alpha_n U_1^*(j\omega) + G_2(j\omega)\alpha_n^2 U_2^*(j\omega) + \cdots + G_n(j\omega)\alpha_2^n U_n^*(j\omega), \end{cases} \tag{3}$$

where $U_n(j\omega)$ represents the n-order nonlinear input of the system and $U^*(j\omega)$ is the spectrum of specific input signal $u^*(t)$, in which $u(t) = \alpha u^*(t)$.

Then, the NOFRFs can be solved by the least squares method as shown in the following equation 4:

$$\begin{aligned} \left[G_1(j\omega), G_2(j\omega), \ldots, G_n(j\omega)\right]^T = &\left\{ \left[\boldsymbol{\alpha}\mathbf{U}(j\omega)\right]^T \boldsymbol{\alpha}\mathbf{U}(j\omega) \right\}^{-1} \\ &\left[\boldsymbol{\alpha}\mathbf{U}(j\omega)\right]^T \mathbf{Y}(j\omega), \end{aligned} \tag{4}$$

where

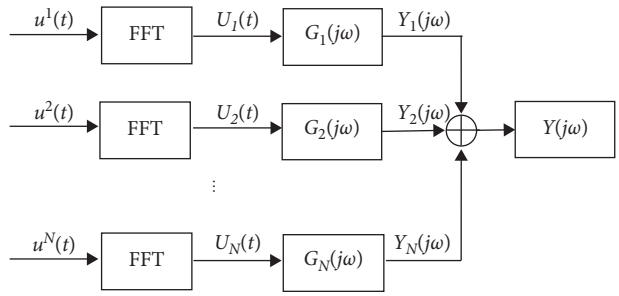

Figure 1: The expression of NOFRFs.

$$\boldsymbol{\alpha}\mathbf{U}(j\omega) = \begin{bmatrix} \alpha_1 U_1^*(j\omega), \alpha_1^2 U_2^*(j\omega), \ldots, \alpha_1^n U_n^*(j\omega) \\ \alpha_2 U_1^*(j\omega), \alpha_2^2 U_2^*(j\omega), \cdots, \alpha_2^n U_n^*(j\omega) \\ \vdots \\ \alpha_n U_1^*(j\omega), \alpha_n^2 U_2^*(j\omega), \ldots, \alpha_2^n U_n^*(j\omega) \end{bmatrix}, \quad (5)$$

$$\mathbf{Y}(j\omega) = \left[Y_1(j\omega), Y_2(j\omega), \ldots, Y_n(j\omega)\right]^T. \quad (6)$$

2.2. Detection Index. Peng et al. [18] integrated the NOFRF values of each order to construct an index Fe with a comprehensive description of the characteristic changes of the nonlinear system, which is defined as

$$\mathrm{Fe}(n) = \frac{\int_{-\infty}^{\infty} \left|G_n(j\omega)\right| \mathrm{d}\omega}{\sum_{i=1}^{N} \int_{-\infty}^{\infty} \left|G_i(j\omega)\right| \mathrm{d}\omega}, \quad 1 \le n \le N. \quad (7)$$

As can be seen from equation (7), the value of Fe(n) is in the range from zero to one. According to the meaning of $G_1(j\omega)$, Fe(1) indicates the linear degree of the system. Meanwhile, Fe(2), ..., Fe(n) could indicate the nonlinear degree of the system, which represents the degree of damage. When the system was subjected to the damage, the ratio of higher-order Fe would increase.

To build a more sensitive index, the concept of information entropy was used. Information entropy can describe the uncertainty of the numerical sequences. The definition of information entropy is

$$H = -\sum_{i=1}^{N} p(x_i) \log p(x_i), \quad (8)$$

where $p(x_i)$ represents the probability of a random variable x_i.

Based on the information entropy theory, the NOFRF entropy index N_E is proposed:

$$N_E = -\sum_{n=1}^{N} \frac{\mathrm{Fe}(n)}{\sqrt{n}} \log\left(\frac{\mathrm{Fe}(n)}{\sqrt{n}}\right). \quad (9)$$

When the ratio of higher-order Fe increased, the value of N_E would increase as well. For damage detection analysis, the value of N_E represents the severity of the damage.

3. Detection of Specimens

3.1. Specimens. In order to verify the effectiveness of the NOFRF entropy-based detection method for structure, a verification experiment was carried out. Four specimens were prepared. The specifications of the specimens are shown in Figure 2 and Table 1. In the preparation of the specimens, the wire cutting was first performed. A wire cut was made in the middle of the specimen, as shown in Figure 2. Then, the surface of it was polished. Finally, three of them were subjected to a three-point bending fatigue loading test to make the prefabricated fatigue cracks.

In order to choose the location of the suspension, the modal shapes of the specimen were analyzed by finite element software ABAQUS. The analysis results are shown in Figure 3. There were different minimum displacement positions in different modes, which are shown as the blue area in Figure 3. The minimum displacement position of each mode was considered comprehensively, and two suspension positions were selected, as shown in Figure 4.

3.2. Harmonic Excitation Detection of Specimens. According to the result of modal analysis of the specimen, the harmonic excitation detection platform is built as shown in Figures 4 and 5. In the platform, the sound vibration sensors could be used to realize both the excitation and acquisition of the given signal. Two sensors were pasted on both ends of the upper surface of the specimen. One of them was used to generate a vibration excitation signal, and the other one was used to acquire the response signal. The specimen was suspended by two rubber bands. The acquisition frequency range of sound vibration sensor is 0–800 kHz. The Tektronix function/arbitrary waveform generator (AFG3022C) is selected to generate a harmonic signal. Finally, both excitation and response signals were collected using the Tektronix mixed domain oscilloscope (MDO3022) at a sampling frequency of 50 kHz.

In order to calculate the first four orders of NOFRFs, four excitation signals with different amplitudes were required. In the experiment, harmonic signals with peak-to-peak values of 7 V, 8 V, 9 V, and 10 V were selected as input, respectively. And the excitation frequency was set to be 8963 Hz, the same as the natural frequency of the second-order modal frequency of the specimen. When the input and

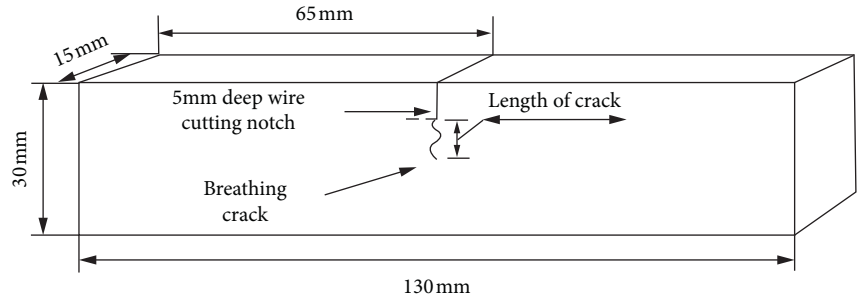

Figure 2: The schematic diagram of specimen.

Table 1: The parameters of specimens.

Parameters of specimen	Value
Size	130 mm × 30 mm × 15 mm
Material	45# steel
Wire cutting depth	5 mm
The diameter of wire-cut wire	0.18 mm
Length of fatigue cracks	0 mm, 3 mm, 10 mm, 15 mm

output data were collected, the values of detection indexes could be calculated through equations (3) and (4). After calculation, the experimental results are shown in Figure 6.

3.3. Hammering Excitation Detection of Specimens. As a comparison with the results of harmonic detection, pulse hammer detection was performed. It had been proved that NOFRFs and the value of N_E index can be well estimated through the pulse hammer detection [19, 20].

In this hammering excitation detection, the detection platform was built as shown in Figure 7. The PULSE Lab shop general test system, 8206-002 impact hammer, 4508 one-way sensor, 3050-a-60 data acquisition module and 3099-a-n1 six-channel analyzer module from B&K Denmark were used in the detection. The sampling frequency was 5 kHz.

The edge excitation signal was collected for 4 times using the force hammer axial hammer test specimen. Four pulse excitation signals with different amplitudes and their response signals were obtained. The least squares method was used to estimate NOFRF of each order as equations (3)–(6). The damage detection index value was calculated through equations (7) and (9). The calculation results are shown in Figure 8.

As can be seen from Figures 6 and 8, under harmonic excitation and hammer excitation, the changes of specimen damage can be directly reflected by the detection indexes N_E and Fe. When the damage became heavier, the value of Fe(1) decreased with the depth of crack, while the values of high-order Fe and the value of N_E increased. It met the theoretical prediction.

Through the above analysis, the validity of the NOFRF entropy-based harmonic detection method was verified.

4. Detection of Pillar Porcelain Insulators

4.1. Experimental Setup and Process. In order to verify the validity of the detection method for damage detection of the pillar porcelain insulator, the harmonic and pulse excitation detection experiments were carried out. Two pillar porcelain insulators were prepared. One of them is without any defect, and the other one has a prefabricated crack inside the flange. The insulator sample is presented in Figure 9.

During the experiments, the insulators were placed vertically on the ground, and the self-weight of the insulators was used to simulate the field installation state of the pillar porcelain insulator. The experimental platform is shown in Figures 10 and 11, respectively. The devices used were the same as mentioned in Section 3.

The single-frequency harmonic excitation signal and the hammer excitation signal were, respectively, used as inputs. And the response signals were collected as output. Then, NOFRFs could be identified, and the nonlinear detection indexes N_E and Fe could be calculated.

In the hammering excitation experiment, the lower flange of the insulator was hammered four times by force hammer from the axial direction. Pulse hammering signals were chosen as input. The response signals were used as output signals. And the input and output signals were collected with a sampling frequency of 5 kHz.

In the harmonic excitation experiment, harmonic signals with peak-to-peak values of 7 V, 8 V, 9 V, and 10 V were selected as input. The frequency of harmonic excitation signal was 1440 Hz which was close to the third modal frequency, and the sampling frequency was 16 kHz. Input and output signals were collected by the Tektronix mixed domain oscilloscope.

The values of detection indexes were calculated as the algorithm described in Section 2.

4.2. Result and Discussion of Experiment. The signal and its frequency spectrum collected from the accelerator in hammer detection are shown in Figure 12.

Then, the NOFRFs were calculated according to equations (3) and (4). The results are shown in Figures 13 and 14.

The frequency spectra of collected signals in harmonic excitation detection are shown in Figure 15.

The results of hammer and harmonic excitation experiments were obtained as shown in Tables 2 and 3, respectively.

From the tables, we can see that in harmonic excitation detection, the relative growth rate of N_E value after damage was 17.59%, while in hammer excitation detection, the

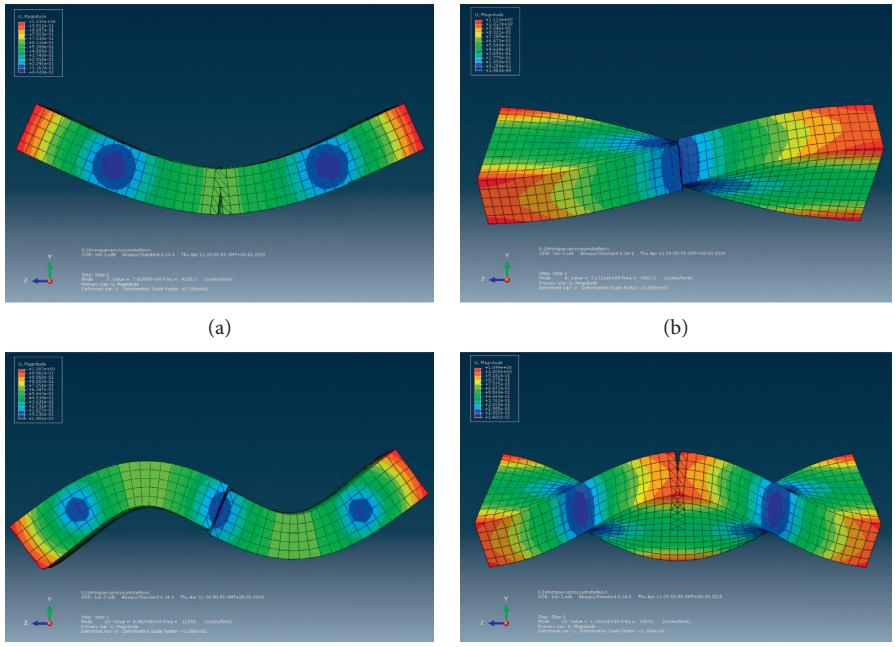

Figure 3: Modal analysis of wire-cut notched metal specimens. (a) The first mode. (b) The second mode. (c) The third mode. (d) The fourth mode.

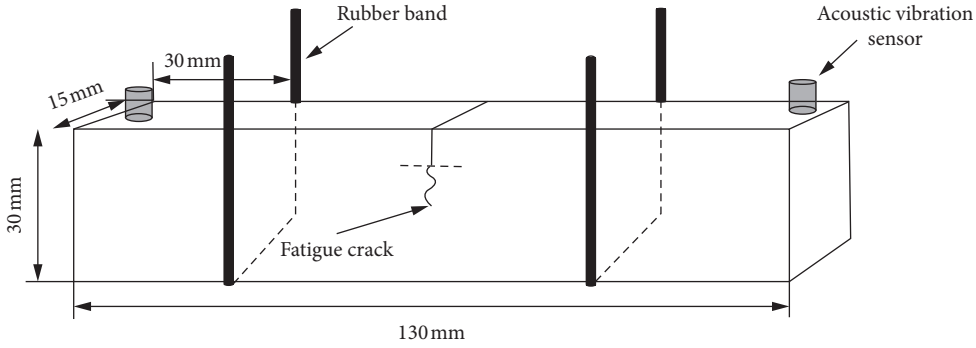

Figure 4: Schematic diagram of metal specimen suspension detection.

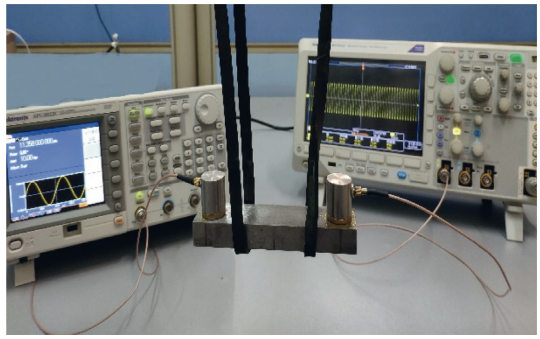

Figure 5: Harmonic excitation detection platform.

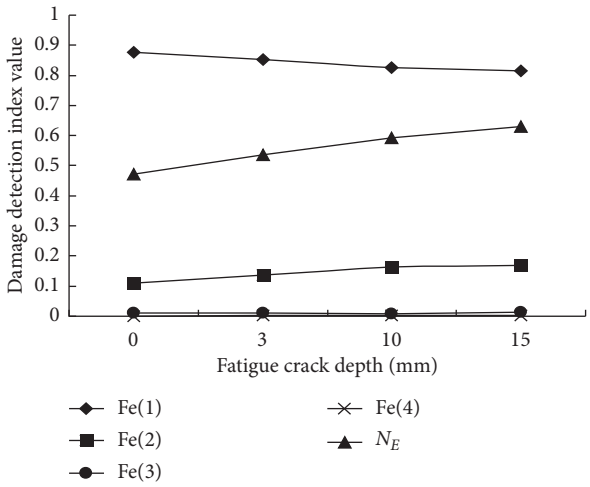

Figure 6: Harmonic excitation damage detection index change curve.

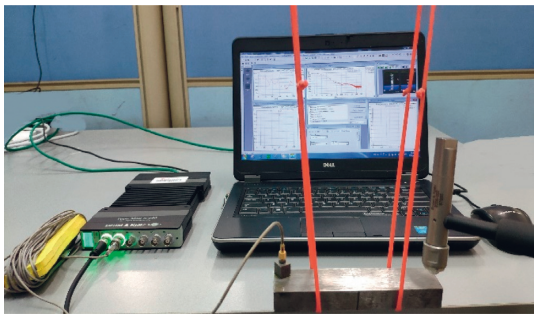

Figure 7: Hammering excitation detection platform.

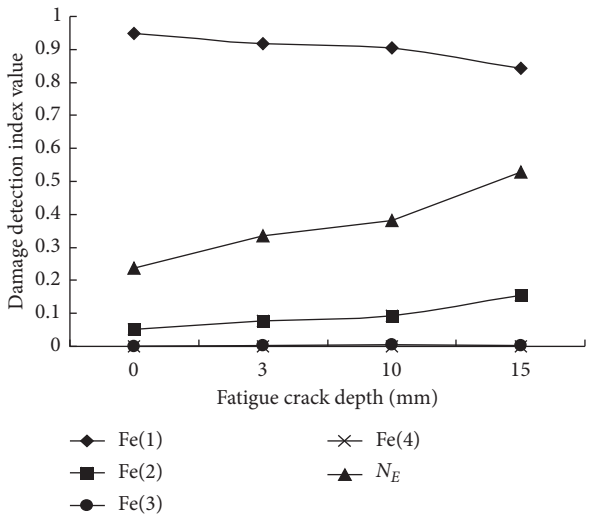

Figure 8: Change curve of damage detection index value under hammer excitation.

relative growth rate of N_E value after damage was 63.35%. It means that the sensitivity of index N_E in hammer excitation detection was higher than that in harmonic excitation detection.

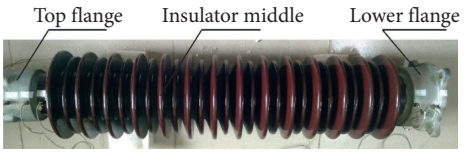

Figure 9: The sample of pillar porcelain insulator.

Figure 10: Harmonic excitation experiment.

Figure 11: Hammering excitation experiment.

Although their sensitivity is different, they can reflect the change of damage of the pillar porcelain insulator.

5. The Influence of Crack Parameters on the NOFRF Entropy Index

The vibration detection is a global detection method, which can detect cracks in almost all locations of the structure. However, different parameters of the crack in the structural system will affect the estimated results of the detection index. In order to investigate the influence degree of different crack parameters on the value of indexes in the detection, a simulation was carried out.

5.1. Simulation Settings. At present, research studies on damage detection of pillar porcelain insulator are mostly focused on the open defect [24]. In this case, the nonlinear contact effect caused by crack opening and closing behavior

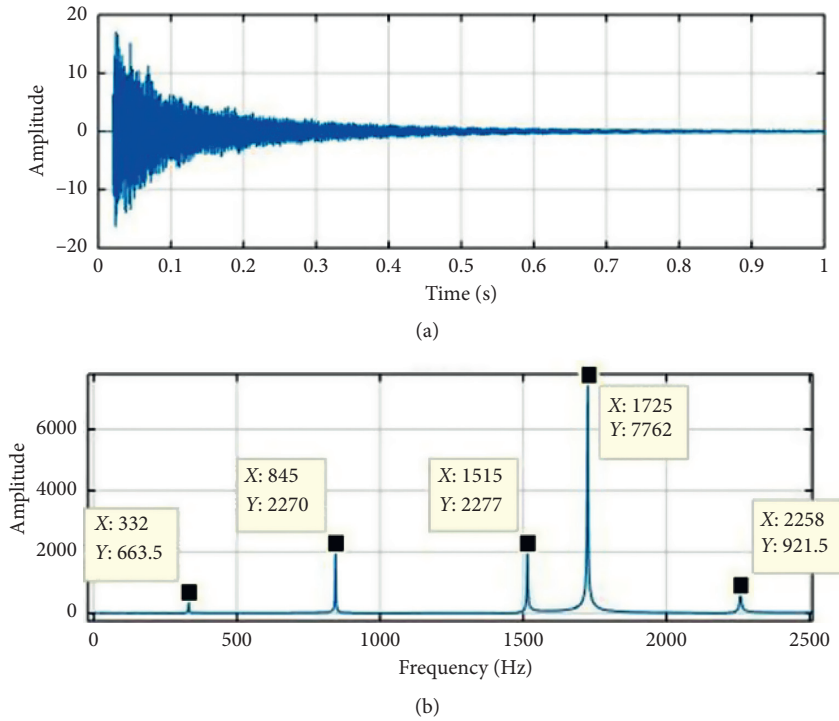

Figure 12: The response signal and its frequency spectrum in hammer detection. (a) The response signal. (b) The frequency spectrum of the response signal.

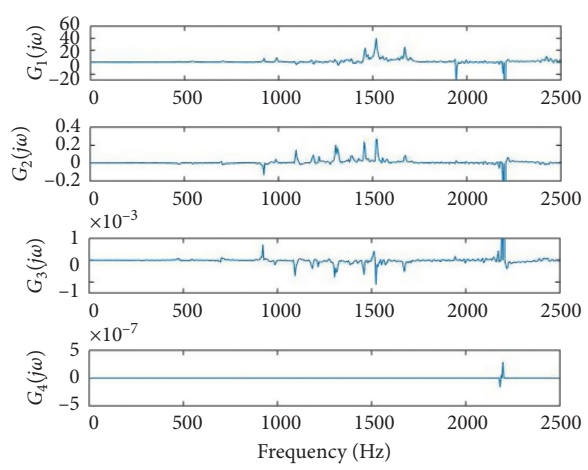

Figure 13: The NOFRFs of healthy pillar porcelain insulator in hammer detection.

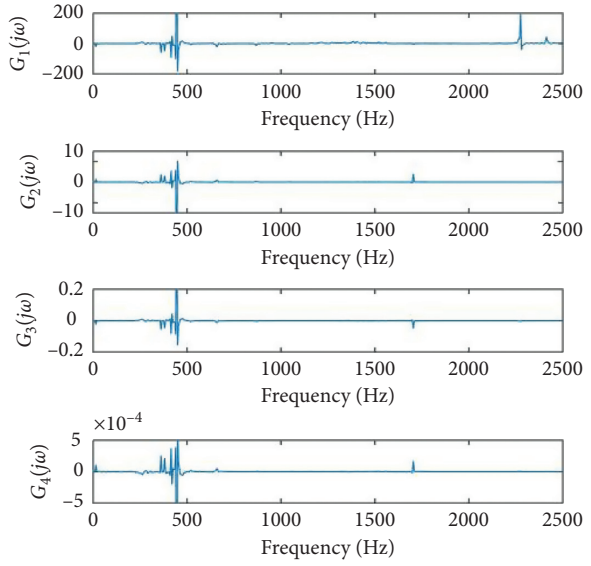

Figure 14: The NOFRFs of cracked pillar porcelain insulator in hammer detection.

would be ignored. Therefore, a representative finite element model of breathing crack should be established. The contact area between two surfaces of the crack changes under the external excitation, and the one-piece combination was similar to the dynamic process of respiration [25].

At first, the 3D model of pillar porcelain insulator was built by SolidWorks as shown in Figure 16. Then, the finite element model of pillar porcelain insulator was imported into ABAQUS. The type of grid element is C3D8R. The material parameters and main dimensions of the pillar porcelain insulator are shown in Tables 4 and 5, respectively.

The breathing crack model was used to simulate the damage of the pillar porcelain insulator. The breathing crack would be set at one of three positions which are I, II, or III in Figure 16. The big umbrellas and small umbrellas are also shown in Figure 16.

The shape of breathing cracks is shown in Figure 17. Δr is the crack depth. L is the crack width.

In ABAQUS, the crack was set in the porcelain body of the insulator model. The noncracked area was bounded by

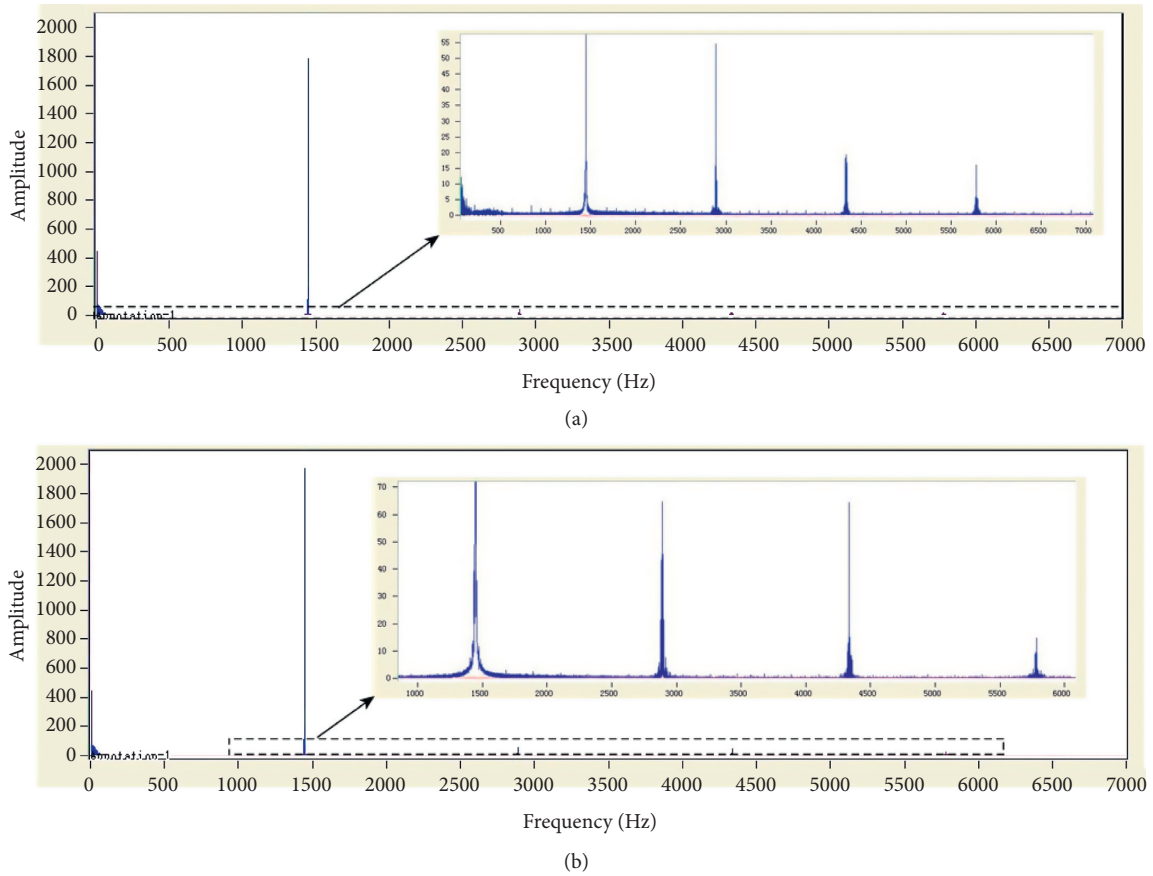

Figure 15: The spectrum of response signal in the harmonic detection. (a) The spectrum of response signal of healthy pillar porcelain insulator. (b) The spectrum of response signal of cracked pillar porcelain insulator.

Table 2: Damage detection index value of pillar porcelain insulator under harmonic excitation.

	Fe (1)	Fe (2)	Fe (3)	Fe (4)	N_E
Healthy	0.85503	0.13411	0.00956	0.00130	0.52484
Prefabricated crack	0.81584	0.17274	0.009691	0.00174	0.61717

Table 3: Damage detection index value of pillar porcelain insulator under hammer excitation.

	Fe (1)	Fe (2)	Fe (3)	Fe (4)	N_E
Healthy	0.95251	0.04695	0.00055	$2.34E-6$	0.21664
Prefabricated crack	0.90988	0.08890	0.00121	$5.10E-06$	0.35388

using the TIE tool. There was no relative motion and deformation between the bounded regions. The two opposing crack areas were set to be the normal hard contact by using the CONTACT tool. Crack faces were set to be independent. The tangential coefficient of friction was set to be 0.5. The Newmark implicit algorithm was used for time integration. When the external load was applied, the dynamic behavior of two crack faces was similar to the breathing action.

5.2. Result and Discussion of Simulation. In order to explore the influences on the N_E value, different conditions were set. Different positions, lengths, and angles of breathing cracks were detected and analyzed through the orthogonal test. In the test, the triangular pulse signal was used as input to excite the pillar porcelain insulator with different conditions which are shown in Table 6. The calculation results are shown in Table 7.

In Table 7, $k1$ is the average value of the factors under level 1, $k2$ is the average value of the factors under level 2, and $k3$ is the average value of the factors under level 3. The range is the difference between the maximum value and the minimum value of the average value.

The result shows that the range of B was larger than that of A, C, and D, which means that the length of breathing crack had the greatest influence on the N_E value among these three factors. The axial angle and location of crack had a little influence on N_E value.

The probability values were obtained by the statistical method of a significance test, which are shown in Table 8. When the probability value of a factor is less than 0.05, the influence of this factor is very significant.

As we can see from Table 8, only the probability value of breathing crack length is less than 0.05, which means that the influence of crack length on the value of index N_E was very significant.

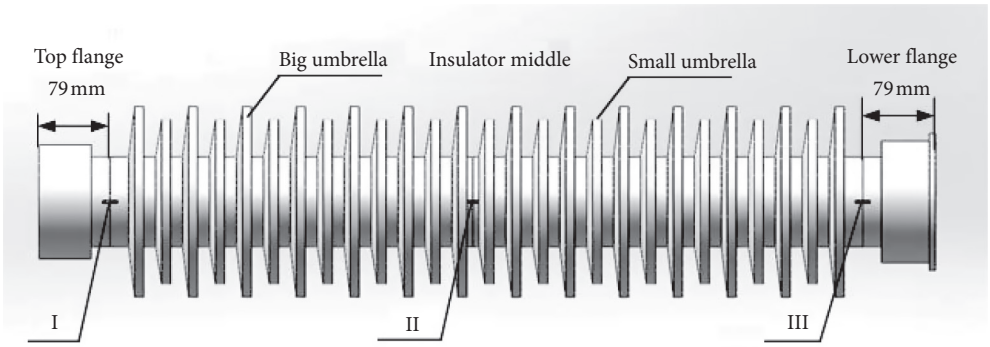

Figure 16: 3D model of pillar porcelain insulator.

Table 4: Material parameters of pillar porcelain insulator.

Material	E (MPa)	Poisson's ratio	Density, t (mm^3)
Porcelain	118000	0.16	$2.6e-9$
Cast iron	175000	0.28	$7.8e-9$
Cement	31000	0.215	$2.3e-9$

Table 5: Main dimensions of pillar porcelain insulator.

Stem diameter (mm)	High (mm)	Big umbrella diameter (mm)	Small umbrella diameter (mm)	Number of umbrellas
59	1175	125	108	27

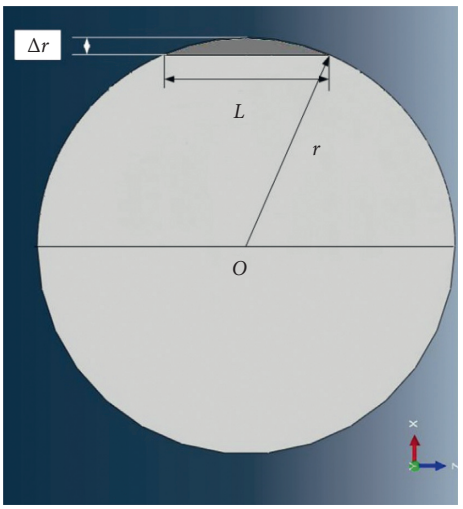

Figure 17: Breathing crack model of pillar porcelain insulator.

Table 6: Factor and level table of the test.

Level	Crack location (A)	Crack length (with fixed depth 5 mm) (mm) (B)	Angle of axial crack (°) (C)
1	Top flange	3	30
2	Insulator middle	5	60
3	Lower flange	15	90

Table 7: Orthogonal test sets and visual analysis.

Number	A (location)	B (mm)	C (°)	D (error term)	N_E
1	1	1	1	1	0.1379
2	1	2	2	2	0.1629
3	1	3	3	3	0.3089
4	2	1	2	3	0.0948
5	2	2	3	1	0.1275
6	2	3	1	2	0.3864
7	3	1	3	2	0.1141
8	3	2	1	3	0.2227
9	3	3	2	1	0.3350
$k1$	0.2032	0.1156	0.2490	0.2001	
$k2$	0.2029	0.1710	0.1976	0.2211	
$k3$	0.2239	0.3434	0.1835	0.2088	
Range	0.0207	0.2279	0.0655	0.0210	

Table 8: Analysis of variance.

Sources of variance	Degrees of freedom	Deviation sum of squares	Mean sum of square	F-crit	Probability value
A	2	0.000869	0.000435	1.30	0.434
B	2	0.084707	0.042353	126.85	0.008
C	2	0.007129	0.003565	10.68	0.086
Error	2	0.000668	0.000334		
Summation	8	0.093373			

6. Conclusion

This paper proposed a NOFRF and information entropy-based harmonic detection method, and several experiments and simulation were carried out. Based on the result of the validation experiment, detection of pillar porcelain insulators, and orthogonal analysis in this paper, the following conclusions can be drawn:

(1) The result of NOFRF entropy index in harmonic detection was similar to the result of hammer detection, which proved that the harmonic detection method can effectively detect and evaluate the damage of the pillar porcelain insulator. Although their sensitivity was different, they can reflect the change of damage of the structural system.

(2) In the orthogonal analysis, the results of NOFRF index under different lengths, positions, and angles of the crack in the structure were obtained. It was found that the crack length was the main factor that affects the detection index.

Data Availability

The data used to support the findings of this study have not been made available because of the laboratory confidentiality agreement.

Conflicts of Interest

The authors declare that they have no conflicts of interest.

Acknowledgments

This study was supported by the Natural Science Foundation of Guangxi (grant nos. 2018GXNSFAA138206, 2018GXNSFAA180116, and 2016GXNSFAA380119), the National Natural Science Foundation of China (grant no. 51365006), and the Manufacturing System and Advanced Manufacturing Technology of Guangxi Key Laboratory Project (contract no. 14-045-15S05).

References

[1] A. Glowacz, W. Glowacz, Z. Glowacz, and J. Kozik, "Early fault diagnosis of bearing and stator faults of the single-phase induction motor using acoustic signals," *Measurement*, vol. 113, pp. 1–9, 2018.

[2] P. Frącz, "System for monitoring partial discharges occurring in overhead power transmission line insulators based on ultraviolet radiation registration," *Insight—Non-destructive Test. Cond. Monit.*vol. 58, pp. 360–366, 2016.

[3] T. Kikuchi, H. Nakauchi, R. Matsuoka, and M. Akizuki, "Remote sensing system for faulty suspension insulator units," in *Proceedings of 5th International Conference on Properties and Applications of Dielectric Materials*, pp. 766–769, Seoul, South Korea, May 1997.

[4] C. B. Geraldo, D. M. Roberto, and C. N. Anselmo, "Experimental estimation of journal bearing stiffness for damage detection in large hydrogenerators," *Shock and Vibration*, vol. 2017, Article ID 4647868, 17 pages, 2017.

[5] J. S. Rapur and R. Tiwari, "On-line time domain vibration and current signals based multi-fault diagnosis of centrifugal pumps using support vector machines," *Journal of Nondestructive Evaluation*, vol. 38, p. 6, 2018.

[6] F. Zhang, S. Ji, Y. Shi, C. Zhan, and L. Zhu, "Investigation on vibration source and transmission characteristics in power transformers," *Applied Acoustics*, vol. 151, pp. 99–112, 2019.
[7] X. Li, H. Guo, and Y. Liu, "Research on damage of porcelain insulator based on vibration detection," *High Voltage*, vol. 45, pp. 101–103, 2009.
[8] A. Bovsunovskii and C. Surace, "Considerations regarding super harmonic vibrations of a cracked beam and the variation in damping caused by the presence of the crack," *Journal of Sound and Vibration*, vol. 288, pp. 865–886, 2005.
[9] U. Andreaus and P. Baragatti, "Experimental damage detection of cracked beams by using nonlinear characteristics of forced response," *Mechanical Systems and Signal Processing*, vol. 31, pp. 382–404, 2012.
[10] S. Smith, G. Wang, and D. Wu, "Bayesian approach to breathing crack detection in beam structures," *Engineering Structures*, vol. 148, pp. 829–838, 2017.
[11] J. Prawin and A. R. M. Rao, "Nonlinear structural damage detection based on adaptive Volterra filter model," *International Journal of Structural Stability and Dynamics*, vol. 18, no. 2, p. 1871003, 2018.
[12] J. Prawin and A. R. M. Rao, "Nonlinear identification of MDOF systems using Volterra series approximation," *Mechanical Systems and Signal Processing*, vol. 84, pp. 58–77, 2017.
[13] L. G. G. Villani, S. da Silva, and A. Cunha, "Damage detection in uncertain nonlinear systems based on stochastic Volterra series," *Mechanical Systems and Signal Processing*, vol. 125, pp. 288–310, 2019.
[14] Z. Q. Lang and S. A. Billings, "Energy transfer properties of non-linear systems in the frequency domain," *International Journal of Control*, vol. 78, no. 5, pp. 345–362, 2005.
[15] Z. K. Peng, Z. Q. Lang, and S. A. Billings, "Resonances and resonant frequencies for a class of nonlinear systems," *Journal of Sound and Vibration*, vol. 300, no. 3–5, pp. 993–1014, 2007.
[16] Z. K. Peng, Z. Q. Lang, S. A. Billings, and G. R. Tomlinson, "Comparisons between harmonic balance and nonlinear output frequency response function in nonlinear system analysis," *Journal of Sound and Vibration*, vol. 311, no. 1-2, pp. 56–73, 2008.
[17] Z. Q. Lang and Z. K. Peng, "A novel approach for nonlinearity detection in vibrating systems," *Journal of Sound and Vibration*, vol. 314, no. 3–5, pp. 603–615, 2008.
[18] Z. K. Peng, Z. Q. Lang, C. Wolters, S. A. Billings, and K. Worden, "Feasibility study of structural damage detection using NARMAX modelling and Nonlinear Output Frequency Response Function based analysis," *Mechanical Systems and Signal Processing*, vol. 25, no. 3, pp. 1045–1061, 2011.
[19] H. Huang, H. Mao, H. Mao et al., "Study of cumulative fatigue damage detection for used parts with nonlinear output frequency response functions based on NARMAX modelling," *Journal of Sound and Vibration*, vol. 411, pp. 75–87, 2017.
[20] H. Mao, W. Tang, Y. Huang et al., "The construction and comparison of damage detection index based on the nonlinear output frequency response function and experimental analysis," *Journal of Sound and Vibration*, vol. 427, pp. 82–94, 2018.
[21] Y. Liu, Y. L. Zhao, J. T. Li, H. Ma, Q. Yang, and X. X. Yan, "Application of weighted contribution rate of nonlinear output frequency response functions to rotor rub-impact," *Mechanical Systems and Signal Processing*, vol. 136, Article ID 106518, 2020.
[22] Y. Liu, Y. Zhao, Z.-Q. Lang, J. Li, X. Yan, and S. Zhao, "Weighted contribution rate of nonlinear output frequency response functions and its application to rotor system fault diagnosis," *Journal of Sound and Vibration*, vol. 460, Article ID 114882, 2019.
[23] Y. Liu, Y. Zhao, J. Li, H. Lu, and H. Ma, "Feature extraction method based on NOFRFs and its application in faulty rotor system with slight misalignment," *Nonlinear Dynamics*, vol. 99, no. 2, pp. 1763–1777, 2020.
[24] C. Zang, Y. Liao, S. Xiao, R. Li, and Q. Wang, "Study on the detection of the defects of pillar insulators by vibration method," *High Voltage*, vol. 49, pp. 8–12, 2013.
[25] F. E. Dotti, V. H. Cortínez, and F. Reguera, "Non-linear dynamic response to simple harmonic excitation of a thin-walled beam with a breathing crack," *Applied Mathematical Modelling*, vol. 40, no. 1, pp. 451–467, 2016.